Raman and fluorescence correlative microscopy in polarized light to probe local femtosecond laser-induced amorphization of the doped monoclinic crystal LYB:Eu

Nicolas Marquestaut, Marc Dussauze, Yannick Petit, Arnaud Royon, Veronique Jubera, Philippe Veber, Michel Couzi, Vincent Rodriguez, Thierry Cardinal, Lionel Canioni

Raman and fluorescence correlative microscopy in polarized light to probe local femtosecond laser-induced amorphization of the doped monoclinic crystal LYB:Eu

Nicolas Marquestaut [a,*], Marc Dussauze [b], Yannick Petit [a,c], Arnaud Royon [a], Véronique Jubera [c], Philippe Veber [c], Michel Couzi [b], Vincent Rodriguez [b], Thierry Cardinal [c], Lionel Canioni [a]

[a] Laboratoire Ondes et Matière d'Aquitaine – UMR 5798 CNRS, Université Bordeaux I, 351 cours de la Libération, 33405 Talence Cedex, France
[b] Institut des Sciences Moléculaires – UMR 5255 CNRS, Université Bordeaux I, 351 cours de la Libération, 33405 Talence Cedex, France
[c] Institut de Chimie de la Matière Condensée de Bordeaux – UPR 9048 CNRS, Chateau Brivazac, Avenue du Dr. Schweitzer, 33608 Pessac Cedex, France

A B S T R A C T

We report on Raman and fluorescence microscopy in polarized light in the oriented Eu^{3+} doped LYB monoclinic crystal after femtosecond laser irradiation. Differential spectra denote large bands typically centered on the pristine glass Raman and fluorescence lines, proving the crystal structure alteration and the significant existence of a laser induced glassy environment of the Eu^{3+} ions inside the laser induced modified zone. Such approach should be annotated for future control of direct laser writing onto biaxial crystals such as LYB:Eu. This is of tremendous interest to probe in situ local modifications, in order to develop new laser induced optical properties in materials for further photonics applications.

1. Introduction

Numerous studies of laser/material interaction above laser induced modification thresholds have been carried out over the past decade, either for undesirable laser induced damages, for example in high power laser systems in relation with material aging and material optical quality, or for profitable laser induced alteration from direct laser writing (DLW) techniques. DLW is at the root of many applications such as the fabrication of micro capillaries for micro fluidics issues, waveguide writing, optical memories, etc. New functionalities based on enhanced optical property modifications can further be developed by tailoring the material chemical composition with photosensitive agents, in order to improve its interaction with the writing laser [1]. Thus, for the laser induced linear properties, DLW can lead to plasmonic enhancement from nanoparticles [2], fluorescence from metallic clusters [3], or oxidation degree modifications of rare earth ions [4]. For the nonlinear properties, second harmonic generation (either from locally buried electric field [5] or from locally laser induced micro crystallization [6]) or third harmonic generation [7] can be obtained.

Most of the studies are related to isotropic material modifications (density change, oxidation degree changes, local crystallization, etc.) [1] while much less refer to laser induced modifications inside crystals, being isotropic [8]or not [9]. Still, laser induced modifications inside a crystal matrix are promising research topics for perennial optical devices and applications, thanks to the intrinsic stability of the crystalline matrix arrangement, but also for waveguide applications for efficient laser and Raman amplification as well as for frequency conversion. Generally, laser induced modifications lead to local index change, local melt, local amorphization or even local recrystallization, giving rise to differential optical properties with respect to the non irradiated bulk matrix.

In this Letter, we study the local modification induced by a femtosecond (fs) near infrared NIR laser on a monoclinic crystal matrix LYB, highly doped with Eu^{3+} rare earth ions. Thanks to point by point optical mapping in both Raman and fluorescence micro spectroscopy in polarized light, we report on the local changes corresponding to partial amorphization of the LYB:Eu crystal, resulting to significant reshaping of the spectral properties in polarized light. The optical specificities of low symmetry crystal optics were properly taken into account, to provide meaningful interpretation of the modified Raman and fluorescence spectra. Such study shows that both Raman and fluorescence spectroscopies are relevant tools to probe soft laser induced modifications and related localized phase transitions, which opens interesting potentiality to further identify the fundamental modifications of the LYB:Eu crystal that could be have as the elementary brick of photonics applications.

2. Monoclinic crystal orientation and associated optical specificities

We considered the $Li_6Y(BO_3)_3$ crystal, grown with the Chockralzki technique under congruent melting, and doped with a 26%

* Corresponding author.
E-mail address: n.marquestaut@loma.u-bordeaux1.fr (N. Marquestaut).

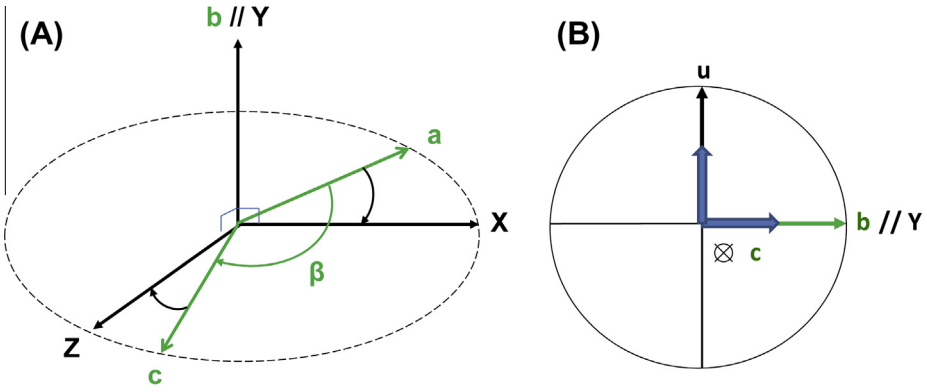

Figure 1. (a) Relative orientation of the crystallographic frame (a–c) and the partially attached dielectric frame (X–Z) in the LYB:Eu monoclinic crystal. (b) LYB:Eu crystal sample orientation under microscope experiments with light propagation direction along the *c*-axis, associated to two polarization eigenmodes respectively parallel or perpendicular to the *b*-axis, thus, respectively parallel to the *Y*-axis or to the u-direction; Blue arrows indicate the polarization directions of the experimental setup described in Figure 2, ensuring the relevant correspondence of both the crystal polarization eigenmodes and the experimental detection directions in polarized light. (For interpretation of the references to color in this figure legend, the reader is referred to the web version of this article).

atomic substitution rate of the Y^{3+} ions by active Eu^{3+} ions, which provided additional linear and nonlinear spectroscopic properties without significant modifications of the initial crystal matrix properties [10,11].

The $Li_6Y(BO_3)_3:Eu^{3+}$ biaxial crystal, hereafter labeled as LYB:Eu, is a centro symmetric crystal that belongs to the {P 2_1/c} monoclinic symmetry group. Its crystallographic frame (a, b, c) is a non orthogonal frame with $a = 0.7157$ nm, $b = 1.6378$ nm, and $c = 0.6623$ nm, and where the monoclinic axis *b* is perpendicular to the (a, c) plane with (a, c) ~105.32° (Figure 1a). Optical propagation properties are optically depicted in the orthonormal dielectric frame (X, Y, Z). Such frame is only partially attached to the crystallographic frame, since monoclinic symmetry issues only impose the dielectric *Y* axis to be collinear to the crystallographic *b* axis, meaning *b*||*Y*. Thus, the plane perpendicular to the monoclinic axis, containing the (*a* and *c*, *X* and *Z*) axes, has a fixed orientation too. However, the orientation of the (X, Z) axes within this plane of monoclinic systems can *a priori* change with any dispersive parameters, as with wavelength for example [12,13]. Here, the four distinct vectors (X, Z) and (a, c) typically verify (a, X) = 39° and (c, Z) = 24° (Figure 1a), in relation with the dielectric frame orientation in the visible wavelength range [14].

The studied LYB:Eu sample was oriented with X ray diffraction and the polished faces were cut perpendicular to the crystallographic *c* axis (Figure 1b). Such orientation ensured the fixed dielectric *b* axis to be parallel to the polished faces. For propagation along the *c* axis in the (X, Z) dielectric plane of the 1 mm thick sample, light can propagate under two polarization eigenmodes, namely the ordinary or extraordinary modes for a polarization being perpendicular or tangent to the (X, Z) plane, respectively. The ordinary polarization mode, which is fixed here parallel to the *b* axis by crystallography properties, is free from spatial walk off while the extraordinary one undergoes double refraction effect [15]. These two polarization modes are thus perpendicular one to each other, whatever any potential orientation dispersion of the dielectric frame, especially when considering UV radiations. Such orthogonal behavior of the polarization modes ensures that one can independently address each polarization mode. Such control of the polarization mode selection independently applies for both the excitation and the collection of optical properties, such as fluorescence or Raman spectroscopy in polarized light, whatever the wavelengths as considered hereafter.

3. Experimental setups

3.1. Direct laser writing

The LYB:Eu crystal sample was irradiated with a NIR fs laser (t Pulse 500 Amplitude Systemes, 500 nJ, 500 fs, 10 MHz, 1030 nm) focused with a microscope objective (100×, NA = 0.7). Laser irradiation above laser induced modification threshold was performed by both adjusting the number of laser pulses and their incident irradiance with an acousto optic modulator. Laser induced modifications were induced at a typical depth of 160 μm below the crystal surface, to reduce the risk of strong surface damage. The laser polarization was adjusted along a fixed polarization mode of the crystal along the considered propagation direction. The following Raman and fluorescence microscopy studies were performed on a spot exposed to 10^5 pulses with an irradiance of about 20 TW cm^{-2}.

3.2. Raman and fluorescence correlative microscopy

We used in this study a combined analysis of (i) μ Raman scattering spectroscopy and (ii) μ fluorescence in back scattering geometry, using the same setup to have access to a direct link between luminescence properties and local structure. The experimental setup is based on a confocal μ Raman HR800 (Horiba/Jobin Yvon) instrument. The same CW laser source at 457 nm linearly vertically polarized was used for both Raman and luminescence studies. The μ Raman spectra were recorded with a typical resolution of 2.5 cm^{-1} using a 600 grooves cm^{-1} grating whereas the μ fluorescence measurements were performed at a spectral resolution of 8 nm using a 150 grooves cm^{-1} grating. Polarized signals were collected with either the parallel or perpendicular configurations, corresponding to incident and scattered lights with collinear or orthogonal polarizations. The objective was a 100× with a numerical aperture of 0.9. Confocal microscopy and motorized XYZ stages allowed 3D investigation.

Considering the crystal sample orientation, the polarization of the CW probe laser was aligned parallel to the *b*//*Y* axis with a propagation direction along the *c* axis (Figure 1b). This geometry prevented any spatial walk off propagation of the excitation laser source, which could have complicated the interpretation of spectral/spatial distributions without providing additional spectroscopic information. The scattered light was collected in back scattering along the *c* axis, and was analyzed in polarized light,

for polarization either parallel to the $b\|Y$ direction or along the u direction, which is perpendicular to Y. These two scattering configurations will be denoted as YY and Yu, respectively, the first Letter corresponding to the incident probe laser polarization and the second one to the selected collection polarization.

4. Results and discussion

4.1. Spectral assignments and laser induced spectral modifications

The crystalline LYB matrix belongs to the monoclinic P21/c (C_{2h}^4) space group, with $Z = 4$ $Li6Y(BO_3)_3$ formula units per primitive unit cell. The structure consists in ortho borate $(BO_3)^3$ groups linked one to another by means of O Y O bridges and with the Li atoms situated in the cavities of this structure [16]. The free $(BO_3)^3$ group is planar, with D_{3h} symmetry, and possesses four normal modes of vibration [17]: the totally symmetric stretching mode ν_1, the out of plane bending ν_2, the antisymmetric degenerate stretching mode ν_3 and the degenerate in plane bending ν_4. The BO_3^3 is situated in general positions in the monoclinic units and consequently all modes of vibration have Raman active components in both the Ag and Bg irreducible representations of the C_{2h} factor group. The Ag and Bg modes are Raman active in the YY and Yu configuration, respectively. As shown in Figure 2, the Raman response is strongly dominated by the Ag component of the ν_1 mode observed as a narrow line (FWHM = 13 cm ^{1}) at 941 cm ^{1} on the YY spectrum. In particular, the Bg counterpart of this mode observed on the Yu (Bg) spectrum is about forty times weaker. The ν_3 modes are attributed to the Raman peaks in the spectral range 1200 1600 cm ^{1}, ν_4 modes are located around 600 cm ^{1} and ν_2 contribution is expected close to 750 cm ^{1} but cannot be discerned in these measurement geometries. At low frequency (below 500 cm ^{1}), the entire sharp Raman peaks are attributed to intermolecular phonon modes.

The emission spectrum of the trivalent Europium Eu^{3+} in the LYB matrix, shown in Figure 3(a), for both YY and Yu configurations is mainly composed of transitions from the $^5D_0$ level towards the fundamental multiplet $^7F_{J(J\ 0-6)}$. The 457 nm excitation wavelength typically corresponds to the edge of the $^7F_0 \rightarrow {}^5D_2$ absorption band of the Eu^{3+}. (typically centered at 466 nm [10]). Emissions from higher levels than the $^5D_2$ one remain weak due to the presence

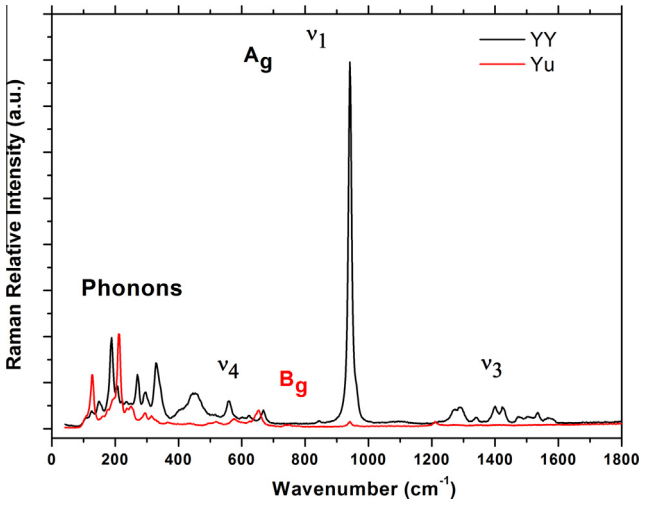

Figure 2. LYB: Eu Raman reference spectra in YY (black line) and Yu (red) polarization configurations. A 10× magnification Zeiss objective was used to prevent Raman excitation from the longitudinal polarization contribution of the probe laser. (For interpretation of the references to colour in this figure legend, the reader is referred to the web version of this article.)

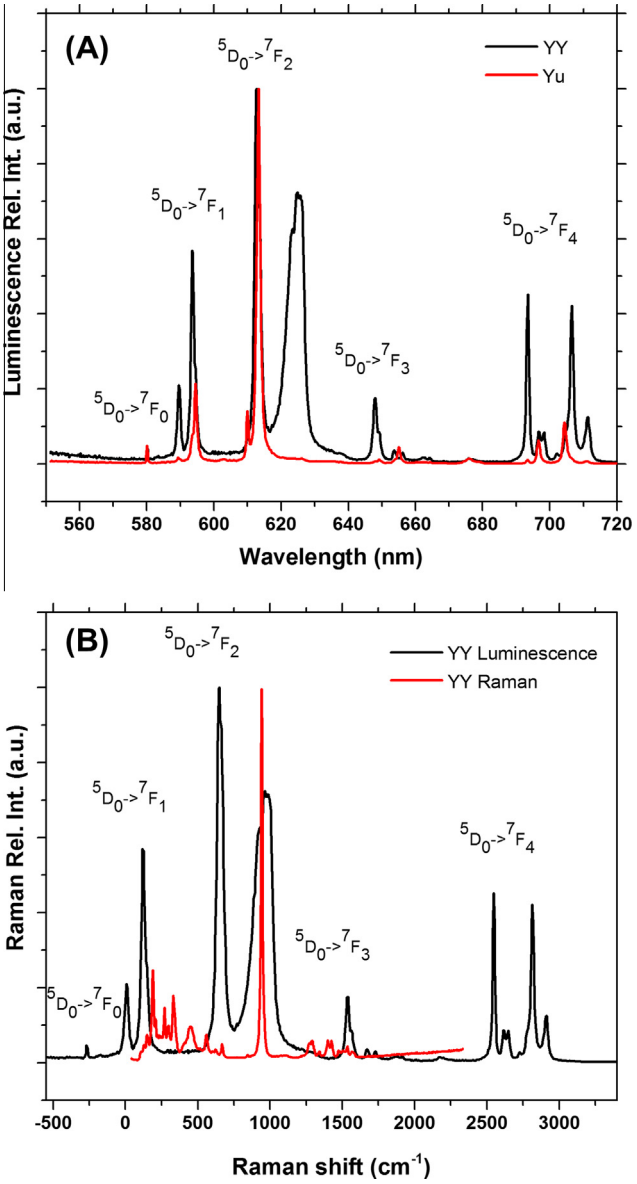

Figure 3. (a) LYB:Eu crystal luminescence reference spectra in YY (black line) and Yu (red) polarization configurations. A 10× magnification Zeiss objective was used to prevent luminescence excitation resulting from the longitudinal polarization contribution of the probe laser. (b) Comparison of the YY Raman spectrum (red line) with the YY luminescence spectral distribution one (black) centered in energy at the 589 nm emission transition (first component of the $^5D_0$—$^7F_1$ magnetic dipole transition). From this last graph, it seems that the observed band peaking at 624 nm is a vibronic type transition which results from the significant coupling of the Eu^{3+} $^5D_0 \rightarrow {}^7F_1$ electronic transition with the strong borate ν_1 vibrational mode. (For interpretation of the references to colour in this figure legend, the reader is referred to the web version of this article.)

of borates groups characterized by strong vibration frequencies, especially at 941 cm ^{1}, leading to the depletion of the $^5D_{J(J>0)}$ levels by non radiative transitions towards the lower level $^5D_0$ by multiphonon process. In addition, for such a doping rate, cross relaxation processes occur between the ^5D_J ($J > 0$) and the fundamental manifold ^7F_J. The $^5D_0$ remains then the unique emitting level. The $^5D_0 \rightarrow {}^7F_0$ transition is in theory, forbidden (from $J = 0$ to $J = 0$), but still it is weakly observable because of the low C1 site symmetry of the Europium ions and also because of $J = 2$ 4 levels wave function correlations. Such single line emission confirms here the existence of a unique site of Eu^{3+} substitution in the LYB matrix. Emission spectra are strongly polarization dependent (Figure 3a).

A large non symmetric band is observed around 624 nm on the YY luminescence. As shown in Figure 3(b), this large band is a vibronic transition associated to the $Eu^{3+5}D_0$ $^7F_1$ magnetic dipole transi tion coupled with the dominant ν_1 borate mode. Therefore, the correlative study of emission and vibration spectra of LYB:Eu en ables us to demonstrate the origin of the vibronic emission and thus to identify all the recorded electronic transitions from this biaxial material. Such explanation of the vibronic emission differs quite significantly to much older results where a similar vibronic transition in LYB:Eu had been proposed to be likely to come from the coupling between the ν_3 borate modes with the $^5D_0$ transition [18].

Raman and fluorescence spectra measured in both pristine crys tal and laser modified zones are depicted in Figures 4 and 5. One should keep in mind that the irradiated zone is 160 μm below the surface. Thus to avoid spatial walk off propagation expected in a general orientation of such a birefringent crystal, all the next optical measurements were carried out for an ordinary polariza tion along the crystal dielectric axis while propagating along the *c* axis, *i.e.* the YY polarization as sketched in Figure 1 [11].

The following data analysis was performed to remove the initial crystalline spectral behavior to that recorded in a laser modified zone, in order to extract and reveal the laser induced resulting spectral responses. Reference spectra from a pure crystalline re gion were subtracted to spectra from laser modified zones. Such analysis required to apply a multiplicative factor to the laser mod ified spectra to properly adjust the relative intensities of spectra being collected from pristine and modified zones. Typically, multi plicative factors of 2 and 1.6 were applied to Raman and lumines cence spectra from the laser modified zone.

The resulting differential spectra denote large bands typically centered close to the pristine crystal Raman and luminescence lines but exhibiting significant frequency shifts and modification of the spectral profiles. The first comment concerns an obvious broadening of all spectral response (both Raman and luminescence emission) within the irradiated zone, evidencing the crystal struc

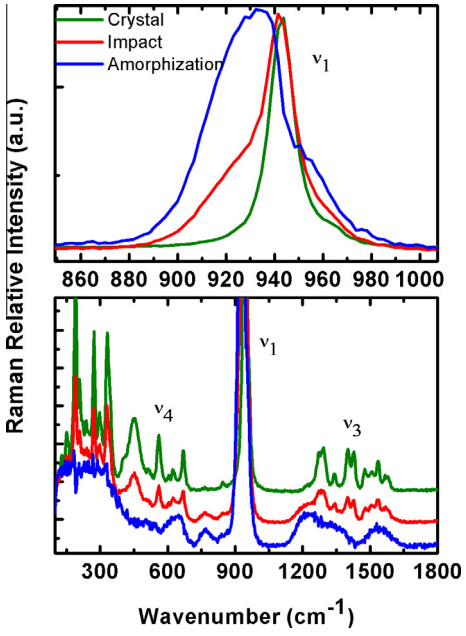

Figure 4. Raman spectra in the YY polarization configuration of pristine crystal (green), laser-modified region (blue) and differential spectrum corresponding to an amorphized spectral signature (red) within (a) the 850–1010 cm^{-1} spectral range focused on the ν_1 normal mode and (b) the 100–1800 cm^{-1} broader spectral range showing ν_2, ν_3 and ν_4 normal modes as well as intermolecular modes. (For interpretation of the references to colour in this figure legend, the reader is referred to the web version of this article.)

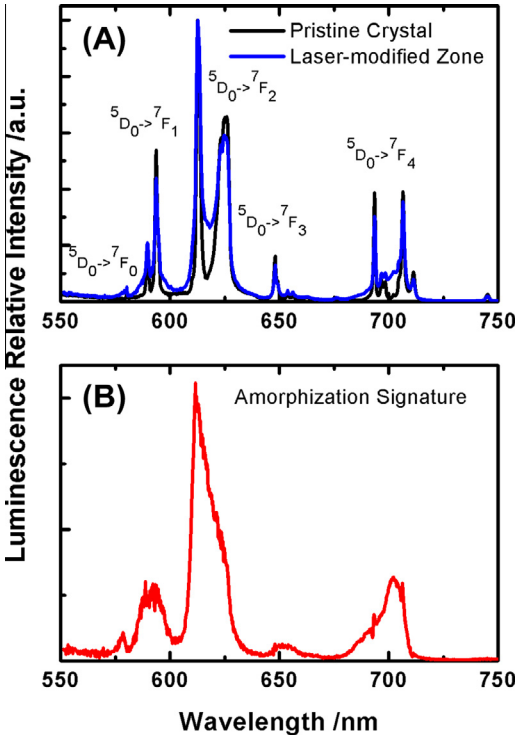

Figure 5. Luminescence spectra in YY polarization configuration for (a) Pristine crystal (black) and laser-modified zone (blue) and (b) the extracted amorphization signature. Reference spectra from a pure crystalline region were subtracted to spectra from laser-modified zones to obtain amorphization signature. (For inter-pretation of the references to colour in this figure legend, the reader is referred to the web version of this article.)

ture alteration and the existence of a laser induced amorphization of the network. Going further into details of the spectral modifica tions of DLW, we observe a significant modification of the ν_1 pre dominant Raman mode starting from a rather sharp band at 941 cm^{-1} in the pristine crystal and going to a broader band shifted at 932 cm^{-1} in the laser modified zone (Figure 4a). Regarding the ν_3 modes, two large envelopes are forming the amorphous spectral signature which intensity profiles denote a gain of intensity at low wavenumbers (1130 1250 cm^{-1}) and an important loss of inten sity in the region 1370 1450 cm^{-1} where were expected two of the main contributions of the ν_3 modes in the crystal. Similar observations can be done in the spectral range of the ν_4 modes, for which the peak at 560 cm^{-1} in the crystal corresponds to a min imum of intensity in the amorphous spectrum. In addition, a new contribution appears at 760 cm^{-1} that can be related to the ex pected ν_2 mode even if not clearly observed in the pristine crystal. To understand these photo induced spectral variations, one should first consider a loss of C_{2h} symmetry due to a local amorphization of the material, which justifies that Raman selection rules have changed. In addition, it is expected that an irradiation induced amorphization may significantly modify boron oxygen bonds inducing thus a set of distortions of the BO_3^3 moieties with initial D_{3h} symmetry to lower symmetries. These considerations are also evidenced in the luminescence spectra where the 4f 4f emission transitions appear strongly broadened in the differential spectrum. The maximum intensity is still related to the electric dipole transi tions which is coherent with a distorted local environment. The overall emission reflects a loss of local symmetry and the overlap of sites distribution around the doping element that can be linked to an amorphous environment of the trivalent Europium. Such spectral broadening of trivalent europium is a well know phenom enon in glass materials and also nano scale materials which pres ent low cristallinity rate [19 20].

4.2. Raman/luminescence correlative imaging of laser modified crystal

In a second step, the spatial distribution of the spectral variations described above has been characterized. In Figure 6, several two dimensional maps of both Raman and luminescence are shown. The first two images correspond to the integrated area of a Raman (or luminescence) peak selectively linked to the crystalline structure (1370 1450 cm ^{1} for Raman and 692 694 nm for luminescence), even after laser induced modification as seen in Figure 4 and Figure 5. In both cases, a clear decrease of intensity is observed within a circle with a diameter of 2 µm (blue zone), with respect to pristine crystal response. One can notice that around the center of the irradiated zone, a less pronounced decrease is observed within a second circular zone with a diameter of 5 6 µm in Raman and could be observed larger in luminescence up to 7 8 µm (green zone). Such larger ring may be attributed to long distance crystal modifications due to thermal expansion and related pressure wave. For the two images in the middle of Figure 6, the integrated area of a Raman (or luminescence) peak selectively linked to the amorphous structure has been selected (1130 1250 cm ^{1} for Raman and 700 705 nm for luminescence). Both Raman and luminescence intensities appear larger within an annular area. This annular domain is particularly clear in the Raman image with an inner diameter of 2 µm and an outer diameter of 5 8 µm. In the last two images, the point to point spectral ratio between amorphous and crystalline Raman (or luminescence) integrated area is depicted. It shows that the relative part of amorphous and crystalline response probed in both spectroscopy techniques is homogeneous within an almost circular area with a diameter in the range of 5 8 µm, much larger than the irradiated voxel during DLW. Finally, before trying to interpret these images, it is important to note that the sizes of the laser affected zones are much bigger than the expected volume of the laser voxel interaction. In our irradiation conditions, such voxel can be considered as a prolate spheroid whose short axis is not bigger than 2 µm while typically considering a linear diffraction limited interaction.

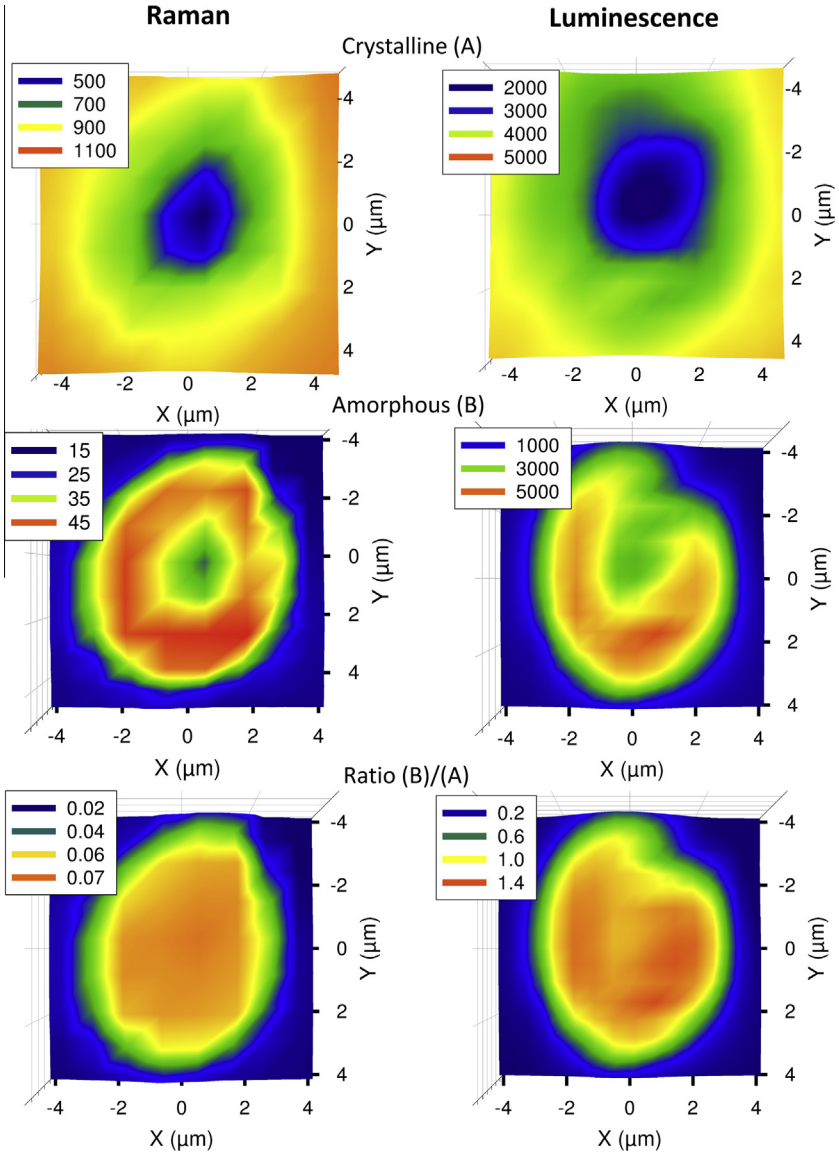

Figure 6. Raman (left side) and luminescence (right side) mapping of the laser-modified zone, The crystalline response have been imaged (upper part) using the integrated area within the spectral range 1370–1450 cm ^{1} for Raman and 692–694 nm for luminescence. The amorphous response have been imaged (middle part) using the integrated area within the spectral range 1130–1250 cm ^{1} for Raman and 700–705 nm for luminescence. The lower part of the figure depicts the relative response of the ratio of integrated areas 'amorphous/crystalline'.

Thus, by combining all these information, one can suspect at least two effects of the laser irradiation on the crystalline material. The first one, as described above in the spectral assignments section, corresponds to an amorphization of the crystal. According to the images of relative Raman (or luminescence) intensities the level of amorphization is homogeneous within a volume much larger than the expected diameter of the laser voxel, as seen in Figure 6 with the remarkable correlation between the structural changes and the fluorescence emission.

The second effect concerns the global intensity decrease in both Raman and luminescence signals which is significant within a volume corresponding to the laser voxel. Such an effect might be linked to a laser induced lower density within the irradiated zone. According to basic thermodynamic considerations, a lower density should be intrinsically induced by the phase change from crystalline to amorphous. In addition, the induced lower density directly imposes an increase of the volume. As the transformation is confined within the bulk of the crystal, laser induced compression zones can be expected at the borders amorphous region. Such considerations could explain the annular shaped enhancements being observed for the amorphous Raman and luminescence responses.

5. Conclusions

We have reported on laser induced permanent modifications in the LYB:Eu monoclinic crystal at the voxel of a tightly focused near infrared femtosecond laser beam. The crystal modifications have been probed by a correlative luminescence and Raman spectroscopy technique under polarized light, providing complementary information on the structural and optical changes. Strong laser induced amorphization of the crystal matrix have been evidenced. An accurate characterization of the spectral variations spatial distribution have shown (i) an homogeneous degree of amorphization within a volume at least two times larger than the laser structuring voxel, and (ii) a variation of density within the amorphous region.

Since the LYB:Eu is a potential laser crystal [21], these observations are of strong interest when considering possibilities to tune both structural and optical properties of this material by direct laser writing, especially for weaker crystal modifications related to waveguide writing for laser amplification applications [12,22–25]. Moreover, since such crystal is a low symmetry crystal, intensity thresholds for laser induced modifications should significantly depend on the considered crystal orientation [12,26]. Finally, such correlative approach provides a versatile tool for micro spectroscopy that can also apply for advanced imaging microscopy to probe wanted DLW but also undesired laser induced damages, in the case of laser material aging.

Acknowledgments

This letter was supported by the French Agency of National Research and the French Aquitaine region.

References

[1] A. Royon, Y. Petit, G. Papon, M. Richardson, L. Canioni, Opt. Mater. Exp. 1 (2011) 866.
[2] A. Podlipensky, A. Abdolvand, G. Seifert, H. Graener, Appl. Phys. A Mater. Sci. Process. 80 (2005) 1647.
[3] M. Bellec, A. Royon, B. Bousquet, K. Bourhis, M. Treguer, T. Cardinal, M. Richardson, L. Canioni, Opt. Express 17 (2009) 10304.
[4] J. Qiu, K. Miura, T. Suzuki, T. Mitsuyu, K. Hirao, Appl. Phys. Lett. 74 (1) (1999) 10.
[5] J. Choi, M. Bellec, A. Royon, K. Bourhis, G. Papon, T. Cardinal, L. Canioni, M. Richardson, Opt. Lett. 37 (2012) 1029.
[6] K. Miura, J. Qiu, T. Mitsuyu, K. Hirao, Opt. Lett. 25 (2000) 408.
[7] L. Canioni, M. Bellec, A. Royon, B. Bousquet, T. Cardinal, Opt. Lett. 33 (2008) 360.
[8] K. Kawamura, M. Hirano, T. Kurobori, D. Takamizu, T. Kamiya, H. Hosono, Appl. Phys. Lett. 84 (2004) 311.
[9] V. Apostolopoulos, L. Laversenne, T. Colomb, C. Depeursinge, R.P. Salathé, M. Pollnau, R. Sellame, G. Cerullo, P. Laporta, Appl. Phys. Lett. 85 (2004) 1122.
[10] V. Jubera, J.-P. Chaminade, A. Garcia, F. Guillen, C. Fouassier, J. Lumin. 101 (2003) 1.
[11] Y. Petit, A. Royon, N. Marquestaut, M. Dussauze, A. Fargues, P. Veber, V. Jubera, T. Cardinal, L. Canioni, Opt. Express 21 (1) (2013) 822.
[12] Born, Wolf, Principles of Optics, Oxford Pergamon press, 1965.
[13] H. Hellwig, J. Liebertz, L. Bohaty, J. Appl. Phys. 88 (2000) 240.
[14] P. Segonds, V. Jubera, J. Debray, B. Ménaert: private, communication (2010).
[15] B. Boulanger, J. Zyss, Chapter 1.7: nonlinear optical properties, Kluwer Academic Publisher, 2003.
[16] G.K. Abdullaev, K.S. Mamedov, Sov. Phys. Crystallogr. 22 (2) (1977) 220.
[17] K. Nakamoto, Infrared and Raman Spectra of Inorganic and Coordination Compounds, 5th ed., J. Wiley, New-York, 1997. 182.
[18] J. Hölsä, M. Leskelä, J. Lumin. 48–49 (1991) 497.
[19] C. Leroy, H. Wang, A. Fargues, T. Cardinal, V. Jubera, M. Treguer-Delapierre, C. Boissière, D. Grosso, C. Sanchez, B. Viana, F. Pellée, Phys. Chem. Chem. Phys. 13 (2011) 11878.
[20] R. Reisfeld, R. Velapoldi, L. Boehm, M. Shalom, J. Phys. Chem. 75 (1971) 3980.
[21] R. Cattoor, I. Manek-Hönninger, J.-C.h. Delagnes, Y. Petit, B. Bousquet, V. Jubera, A. Fargues, Ph. Veber, M. Velazquez, A. Garcia, L. Canioni, Proc. SPIE 8235 (2012) 82351A.
[22] F. Bain, A. Lagatsky, R. Thomson, N. Psaila, N. Kuleshov, K. Kar, W. Sibbett, C. Brown, Opt. Express 17 (2009) 22417.
[23] J. Siebenmorgen, K. Petermann, G. Huber, K. Rademaker, S. Nolte, A. Tünnermann, Appl. Phys. B 97 (2009) 251.
[24] S. Beecher, R. Thomson, D. Reid, N. Psaila, M. Ebrahim-Zadeh, A. Kar, Opt. Lett. 36 (2011) 4548.
[25] A. Ródenas, A. Nejadmalayeri, D. Jaque, P. Herman, Opt. Express 16 (2008) 13979.
[26] Y. Petit, S. Joly, P. Segonds, B. Boulanger, Laser Photon. Rev. 1–18 (2008). 10.1002/lpor.201200078.